Journal of Electrical Engineering, Vol. 75, No. 2, 2024, pp. 166-172

sciendo

PAPERS

Stability and reliability analysis for broadband current array sensing system applied to GIS

Fei Du, Hao Yu, Shuai Yuan, Jiangang Bi, Dehui Fu

In order to further improve the defect detection capability of gas insulated switchgear and avoid equipment faults, broadband current array sensing system is designed to simultaneously monitor the system status such as partial discharge, relative dielectric loss, and power frequency overvoltage. The dynamic model of the system is analysed, and based on which, the system state equation is obtained meanwhile fault observer is designed, and the system stability criterion under $H\infty$ condition is calculated. The reliability of the system under different packet loss rates is verified based on cloud models, and the principle of using appropriate electromagnetic compatibility to prevent packet loss rates below 50% is proposed.

Keywords: gas insulated switchgear, current sensing, stability, reliability, system control

1 Introduction

With the increasing reliability requirements for Gas insulated switchgear (GIS), the demand for online monitoring and sensing reliability is also increasing [1]. However, conventional partial discharge (PD) sensing methods such as ultrasound and ultra-high frequency are independent and all indirect measurements, making it difficult to directly reflect the serious state of internal defects in the equipment. Due to the lack of a unified sensing system, it is difficult to achieve system integration [2-4].

Broadband Current Array Sensing System (BCASS) is used for online monitoring of power equipment, which can achieve important states such as PD and dielectric loss of power equipment during operation by measuring the current at different frequencies of the equipment position. BCASS utilizes wired and wireless methods for sensing data transmission, analysis result transmission, and sensor measurement feedback control [5-7]. Wireless sensor networks are deployed in substation environ-ments, and routing is an important component of wireless sensor networks. The performance of routing is directly related to the timeliness and accuracy of information collection. Given that wireless sensor networks are limited by communication capabilities, number of nodes, node power consumption, and operating modes, the quality of routing work is prone to decrease with sudden changes in substation conditions and changes in sensor array topology. The routing algorithm used in array sensing systems (networks) needs to maintain functional stability after changes in operating conditions and topology. The traditional logic of judging stability is limited to the range of threshold, existence of analytical solutions, and clear boundary conditions, resulting in the inability to accurately define the specific concept of sensor network routing stability when substation conditions and sensor network control laws are complex [8-10]. Therefore, the concept of cloud model is introduced when evaluating the stability of sensor network routing.

In this paper, the dynamic model of current array sensing system used in on-line monitoring of GIS is established. The types of monitored current include but not limited to high-frequency PD, large overvoltage current, iron core grounding current, bushing end screen current. A stable control system is designed for the adaptive fault observer of uncertain linear time invariant (LTI) systems, based on which, the cloud mode is proposed, and the stability of different routing algorithms is calculated to guide the design of BCASS applied to GIS devices.

2 Stability of BCASS applied to GIS

2.1 Sensor layout and current types

The system dynamic model of broadband current sensor array for GIS equipment is composed of input, sensor response, AD conversion, data transmission and feature extraction. The inputs include GIS CB grounding copper large power frequency current $i_{\text{L-GCB}}$, GIS CB grounding copper high frequency partial discharge current $i_{\text{pd-GCB}}$, GIS CB grounding copper large over-voltage current $i_{\text{O-GCB}}$, GIS CT CB in-phase current

China Electric Power Research Institute, No.15 Qinghe Xiaoying East Road, Haidian District, Beijing, China
dufei@epri.sgcc.com.cn

https://doi.org/10.2478/jee-2024-0020, Print (till 2015) ISSN 1335-3632, On-line ISSN 1339-309X

busbar large power frequency current $i_{\text{L-GCB-PT}}$, GIS CT-CB in-phase current busbar high frequency partial discharge current $i_{\text{pd-GCB-PT}}$, GIS-CT grounding copper large power frequency current $i_{\text{L-GPT}}$ .The specific installation positions and groups of various current sensors are shown in Fig. 1.

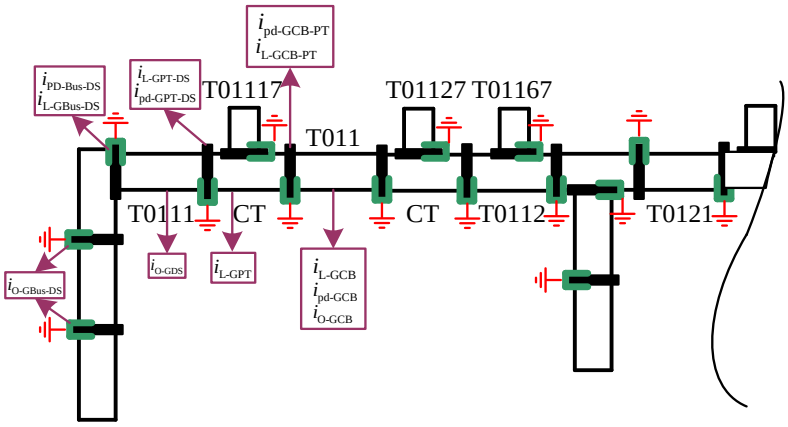

Fig. 1. Sensor layout and corresponding current types of BCASS

2.2 Dynamic model

The BCASS interpretation model for GIS includes two feedback loops, which is shown in Fig. 2. The first is the circuit breaker overvoltage feedback loop. When the circuit breaker generates high-frequency high current in the grounding bar due to operation, fault, etc., the feedback loop starts, triggering high-frequency partial discharge and power frequency phase measure-ment again; The second is the bus overvoltage feedback loop. When overvoltage occurs due to line action, main transformer fault, or internal GIS fault, the feedback loop is activated to achieve interval (string) identification, activate all current sensors of the corresponding string or interval, and re-evaluate the operating status of the interval. The calculation of the status of GIS circuit breakers, isolating switches, and busbar is as follows:

$$y_G = \begin{bmatrix} F_{\text{CB}}(f_i, A_i, \varphi_i) \\ F_{\text{DS}}(f_i, A_i, \varphi_i) \\ F_{\text{Bus}}(f_i, A_i, \varphi_i) \end{bmatrix} \begin{bmatrix} \dot{y}_{\text{GCB}} \\ \dot{y}_{\text{GDS}} \\ \dot{y}_{\text{GBus}} \end{bmatrix}^T . \tag{1}$$

Here, $\dot{y}_{\text{GCB}}$,$\dot{y}_{\text{GDS}}$ and $\dot{y}_{\text{GBus}}$ are the status of circuit breakers, isolating switches, and busbar respectively.

$$\dot{y}_{\text{GCB}} = \begin{bmatrix} H_{\text{L-I}}H_{\text{L-AD}} \\ H_{\text{H-i}}H_{\text{H-AD}} \\ H_{\text{H-I}}H_{\text{H-AD}} \\ H_{\text{L-I}}H_{\text{L-AD}} \\ H_{\text{H-i}}H_{\text{H-AD}} \\ H_{\text{L-I}}H_{\text{L-AD}} \end{bmatrix}^T \left(\begin{bmatrix} i_{\text{L-GCB}} \\ i_{\text{pd-GCB}} \\ i_{\text{O-GCB}} \\ i_{\text{L-GCB-PT}} \\ i_{\text{pd-GCB-PT}} \\ i_{\text{L-GPT}} \end{bmatrix} + N \right) \tag{2}$$

$$\dot{y}_{\text{GDS}} = \begin{bmatrix} H_{\text{L-I}}H_{\text{L-AD}} \\ H_{\text{H-I}}H_{\text{H-AD}} \\ H_{\text{L-I}}H_{\text{L-AD}} \\ H_{\text{L-I}}H_{\text{L-AD}} \\ H_{\text{H-i}}H_{\text{H-AD}} \\ H_{\text{L-I}}H_{\text{L-AD}} \\ H_{\text{H-i}}H_{\text{H-AD}} \end{bmatrix}^T \left(\begin{bmatrix} i_{\text{L-GCB-PT}} \\ i_{\text{pd-GCB-PT}} \\ i_{\text{L-GPT}} \\ i_{\text{L-GPT-DS}} \\ i_{\text{pd-GPT-DS}} \\ i_{\text{L-GBus-DS}} \\ i_{\text{PD-Bus-DS}} \end{bmatrix} + N \right) \tag{3}$$

$$\dot{y}_{\text{GBus}} = \begin{bmatrix} H_{\text{L-I}}H_{\text{L-AD}} \\ H_{\text{H-i}}H_{\text{H-AD}} \\ H_{\text{H-I}}H_{\text{H-AD}} \\ H_{\text{H-I}}H_{\text{H-AD}} \end{bmatrix}^T \left(\begin{bmatrix} i_{\text{L-GBus-DS}} \\ i_{\text{PD-Bus-DS}} \\ i_{\text{O-GBus-DS}} \\ i_{\text{O-GDS}} \end{bmatrix} + N \right) \tag{4}$$

2.3 Stability criteria and fault-tolerant control

In order to maintain the stable operation of BCASS, an adaptive fault observer is designed for uncertain LTI systems, and a stability (i.e. fault-tolerant) control system is designed. Firstly, an improved Adaptive Fault Estimation Algorithm (AFEA) is proposed, which utilizes stability theory and generalized inverse matrix theory to enhance the algorithm's speed and accuracy. An analysis of the convergence interval and convergence rate is introduced to determine the unknown parameters in the fault estimation model. Then, based on the improved Adaptive Fault Estimation Observer (IAFEO), an observer-based State Feedback Fault Tolerance Controller (OSFFTC) is constructed.

For any LTI system state equation:

$$\begin{cases}\dot{x}(t) = Ax(t) + Bu(t) + Ef(t) + DN(t) \\ y(t) = Cx(t)\end{cases} \quad (5)$$

When a time-varying fault occurs in the system, the first-order derivative of the fault with respect to time $\dot{f}(t)$ exists and the norm of $f(t)$、$\dot{f}(t)$ is bounded, namely the existence of positive real numbers f_0, f_1 makes $||f(t)||_2 \le f_0, ||\dot{f}(t)||_2 \le f_1$ valid. Therefore, the stability criterion can be derived as follows.

For a given circular area $D(\lambda, \tau)$ and scalar $\gamma > 0, \sigma > 0$, if the symmetric positive definite matrix $P \in R^{n\times n}$ and symmetric matrix $R_1 \in R^{r\times r}$ make the following equation hold true, IAFEO can distribute the eigenvalue of $(A - LC)$ within the unit circle $D(\lambda, \tau)$, and meet performance indicators H_∞ ($||\tilde{e}(t)||_2 < \gamma||\tilde{N}(t)||_2$), the Gain Matrix of IAFEO can be set as $L = P^{-1}Y$.

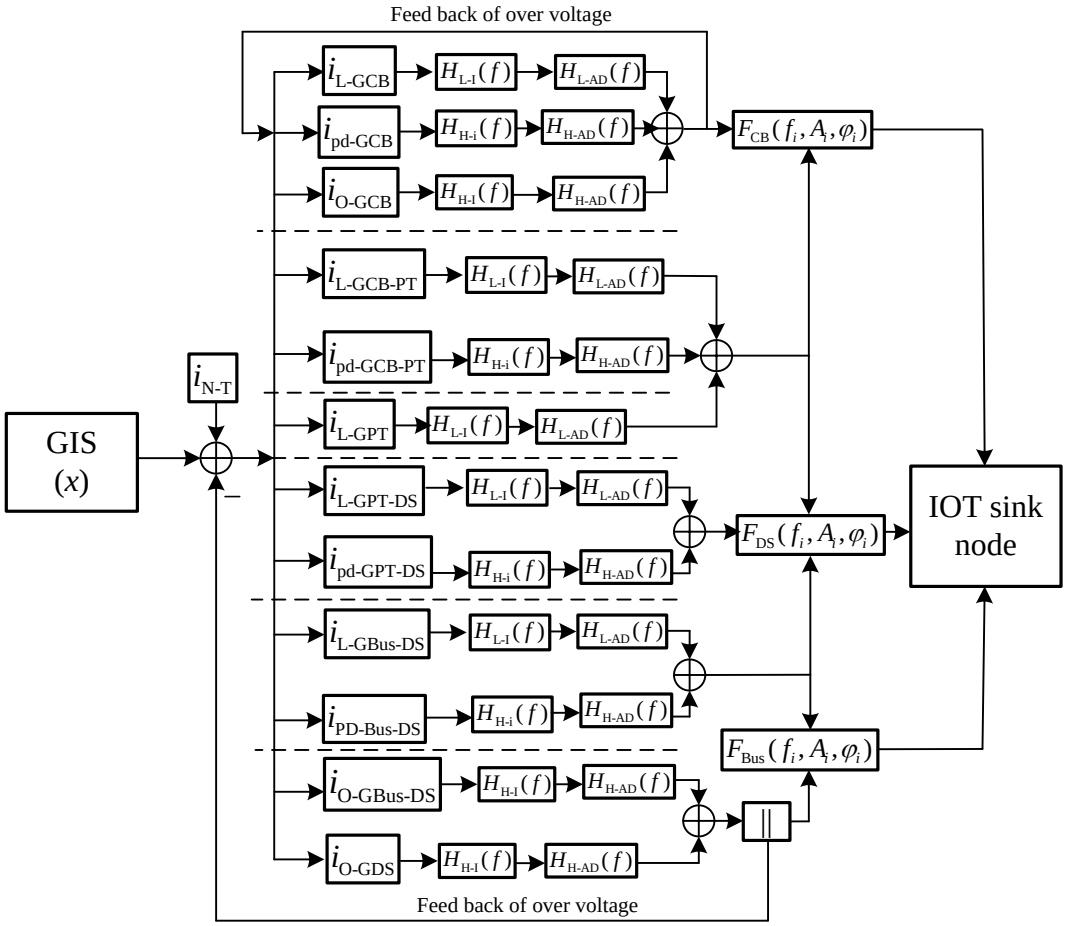

Fig. 2. Sensor layout and corresponding current types of BCASS

IAFEO ensures that $(e_x(t), e_f(t))$ converges to the interval at a rate greater than $e^{-\alpha t}$. To further calculate stability criteria, the Lyapunov function is introduced as follows.

$$\begin{cases} V \le \lambda_{\max}(P)\,\|e_x(t)\|_2^2 + \dfrac{1}{\sigma}\|e_f(t)\|_2^2 \le \max\left[\lambda_{\max}(P), \dfrac{1}{\sigma}\right](\|e_x\|_2^2 + \dfrac{1}{\sigma}\|e_f\|_2^2) \\ \dot{V}(t) \le -\alpha V(t) + \varepsilon \end{cases} \quad (6)$$

If $(e_x(t), e_f(t)) \in \bar{S}$ and $\dot{V} \le 0$, the trajectory of $(e_x(t), e_f(t))$ in outside is continuously approaching the set *S*. When $\sigma > \frac{1}{\lambda_{max}}$, the stability condition of BCASS is shown in equation (7).

$$\begin{cases} \alpha = \dfrac{min(b_1, b_2)}{\lambda_{max}} \\ b_1 = \lambda\left(Q - \dfrac{1}{\mu_1}PDD^TP - \dfrac{\mu_2}{\sigma}(A-LC)^T(A-LC)\right)_{min} \\ b_2 = \lambda\left(\dfrac{2}{\sigma}E^TPE - \dfrac{2}{\sigma}R_1 - \dfrac{1}{\sigma\mu_2}E^TPPE - \dfrac{1}{\sigma\mu_3}E^TPDD^TPE - \dfrac{1}{\sigma\mu_4}R_1^2 - \dfrac{1}{\sigma\mu_5}I_r\right)_{min} \end{cases} \tag{7}$$

An arbitrary relaxation system is defined as bounded input-bounded output stable. For LTI systems, the necessary and enough conditions for the stability can be defined as equation (8)

$$\sum_{n=-\infty}^{\infty} |h(n)| < \infty \tag{8}$$

For causal system transfer function $h(n)$, the Z-transform is defined as equation (9)

$$H(z) = \sum_{n=-\infty}^{+\infty} h(n)z^{-n} \tag{9}$$

Therefore, when the unit circle ($|z|$=1) is contained in the convergence domain of $H(z)$, the LTI system is stable. The pole-zero plot of broadband current sensing array system are calculated, as shown in Fig. 3.

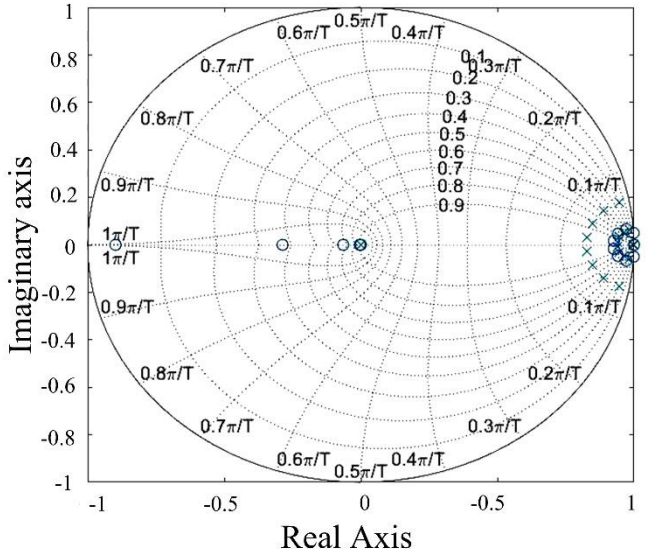

Fig. 3. Pole-zero plot of broadband current sensing array system

The system transfer function consists of 9 pairs of conjugate poles: 0±0i, 0.831±0.031i, 0.850±0.089i, 0.890±0.141i, 0.940±0.012i, 0.941±0.177i, 0.949±0.033i, 0.964±0.050i, 0.986±0.061i. All poles are within the unit circle, namely, the convergence domain of the system contains the unit circle, which indicates that the system is stable.

3 Reliability of BCASS applied to GIS

3.1 Routing stability indicators

From the perspective of BCASS operation, considering node packet loss rate, number of sensors installed on nodes, unstable factors or faults during data packet transmission can lead to abnormal array sensor output results. Therefore, the routing stability of wireless sensor networks mainly includes three aspects: network conditions, average energy consumption, and network communication success rate.

The network conditions N_C including disturbances in the network environment and calculation methods during stability analysis, such as node loss rate and node failure. The average energy consumption E_{dave} includes the total energy consumed by each sample node to transmit one data packet to its superior/subordinate nodes. The success rate of network communication *S*r is defined as the ratio of the total number of data packets received by the upper/lower nodes to the total number of data packets sent by the same source nodes when the sample node sends a set of data packets to the upper/lower nodes as the source node.

For data centric wireless sensor networks, the reliability and immediacy of data transmission are the core issues in engineering, and the routing algorithm of wireless sensor networks plays a crucial role in data transmission. One of the concerns for operators is whether the routing algorithm can maintain stability in the event of external environmental changes and self-disturbances. Therefore, the focus of this project's research on routing stability is on the stability of routing data transmission, which mainly examines key factors that affect communication success rate, such as packet loss rate, the delay of base station receiving data packets, and the number of data packets. The routing stability is defined into four levels through language variables:

C1 level, with excellent reliability, indicating that the array sensing system can automatically recover to normal in the event of significant disturbances (such as

electromagnetic interference or temporary disconnection of communication nodes).

C2 level, with good reliability, indicating moderate anti-interference ability. For example, the array sensing performance temporarily decreases under electromagnetic interference, requiring short-term manual maintenance.

C3 level, reliable, indicating low immunity, such as reduced performance under electromagnetic interference, requiring long-term or short-term manual mainte-nance, resulting in reduced performance.

C4 level, poor reliability, indicating no immunity, such as direct damage to equipment under electromagnetic interference.

Reliability evaluation is divided into qualitative evaluation and quantitative evaluation according to cloud models. Qualitative evaluation is the mapping from stability space to stability space, while quantitative evaluation is the mapping from stability space to stability space. The 4-level reliability mapping relationship is defined as follows:

$$\begin{cases} C_1 \rightleftharpoons c \in (0.8,1] \\ C_2 \rightleftharpoons c \in (0.6,0.8] \\ C_3 \rightleftharpoons c \in (0.4,0.6] \\ C_4 \rightleftharpoons c \in [0,0.4] \end{cases} \tag{10}$$

3.2 Routing stability inference rules based on two-dimensional cloud model

In the case of high packet loss rate in routing algorithms, if the array sensor network can still maintain a high success rate, it is obvious that the reliability of the array sensor network is C1, which means that routing stability cannot be measured solely from packet loss rate or a certain dimension. The routing stability inference rules of two-dimensional cloud model are represented as in Eqn. (11).

$$r_{ij}: \left(x_1 = A_i \& x_2 = B_j\right) \rightarrow y = C_k \tag{11}$$

Here, r_{ij}, x_1, x_2, y represent the inference rules, input and output respectively, A_i and B_j are the input rule prerequisites for cloud models, C_k is the result. x_1 and x_2 are Input to cloud generator $P_{Ai,Bj}$ and the corresponding membership degree $\mu_{ij,P}$ is obtained. The max membership degree μ_{max} is calculated by rule selector, and the corresponding reliability level. The flow chart of the rule selector is shown in Fig. 4.

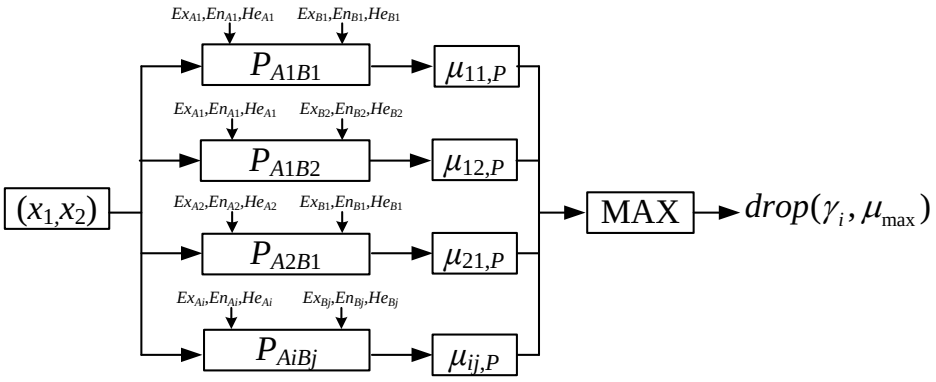

Fig. 4. Flow chart of the rule selector

3.3 Reliability verification

To verify the reliability of BCASS in unicast routing, multicast routing, and tree routing networking scenarios, different node packet loss rates, communication success rate tests are conducted on three routing method. Each routing method is tested 10 times for each packet loss rate, with a nodes' packet loss rate of 50% as an example. The results are shown in Table 1.

Table 1. The network communication success rates

Method	#1	#2	#3	#4	#5	#6	#7	#8	#9	#10
Unicast routing	0.016	0.097	0.086	0.049	0.080	0.014	0.042	0.092	0.079	0.086
Multicast routing	0.166	0.104	0.095	0.093	0.068	0.076	0.074	0.039	0.066	0.007
Tree routing	0.471	0.403	0.338	0.365	0.360	0.462	0.359	0.232	0.395	0.313

According to section 3.2, reliability of each kind of routing with different packet loss rate is calculated, as shown in Table 2.

Table 2. The network communication success rates

Method	Parameter	Node's Packet loss rate				
		10%	20%	30%	40%	50%
Unicast routing	success rate of communication	0.47	0.26	0.17	0.08	0.06
	Reliability level/Membership degree	C_{41}/0.32	C_{42}/0.14	C_4/0.25	C_4/0.56	C_4/0.37
	Reliability	0.30	0.05	0.10	0.26	0.28
Multicast routing	success rate of communication	0.60	0.33	0.21	0.10	0.08
	Reliability level/Membership degree	C_3/0.82	C_{32}/0.48	C_4/0.12	C_4/0.46	C_4/0.35
	Reliability	0.48	0.41	0.15	0.28	0.29
Tree routing	success rate of communication	0.93	0.81	0.72	0.47	0.34
	Reliability level/Membership degree	C_{12}/0.51	C_{12}/0.85	C_{11}/0.31	C_{31}/0.23	C_{31}/0.20
	Reliability	0.81	0.83	0.95	0.60	0.49

According to Table 2, when the packet loss rate is less than 50%, tree routing can achieve a higher network communication success rate. Further calculation of 2-D cloud model formed by the accuracy of the tree routing and packet loss rate stability is shown in Figure 5.

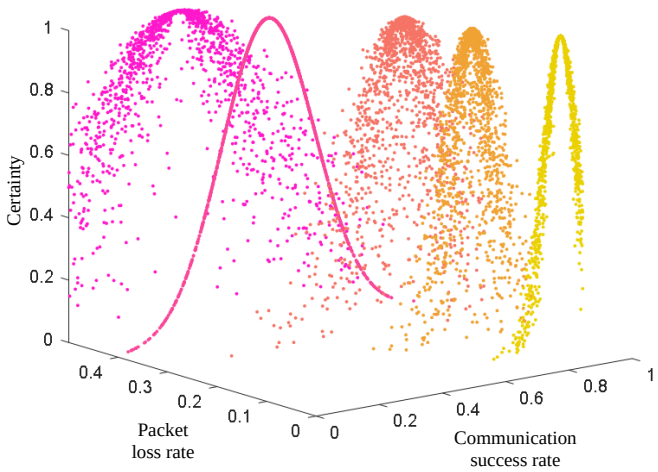

Fig. 5. 2-D cloud model of tree routing's reliability

According to the 2-D cloud model of the tree routing, when there is a certain packet loss rate, the uncertainty and communication success rate approximate a normal distribution, indicating a steady-state stochastic process characteristic. When the packet loss rate is 0.1, the cloud space with a certainty of 0.5 has a width of about 0.15 and a thickness of about 0.01, indicating that the communication measured at this packet loss rate is more reliable and has higher credibility. Specifically, when the packet loss rate is 0.4, the cloud droplet thickness reaches its minimum value, but the width is larger than when the packet loss rate is 0.1-0.3, which indicates that the super entropy of the communication success rate is lower, the test results are more reliable, but the entropy value is larger, and the evaluation results have a wide range of levels. During on-site application, the packet loss rate should be avoided to reach 50%, that is, adding electromagnetic shielding measures to routing and communication hardware, and reducing communication distance.

4 Conclusion

A BCASS design method for GIS current monitoring is proposed. Based on the system dynamics model of BCASS, the state equation is proposed, and the system stability criterion is calculated by designing a fault observer. The state feedback fault-tolerant controller of the observer makes BCASS have strong stability and convergence speed. On the basis of the $H\infty$ condition of stability, 9 pairs of poles of the system are calculated, all located within the unit circle, verifying the stability of the system in design. In order to conduct reliability testing of BCASS in practical engineering, a reliability testing method based on cloud model theory is established using packet loss rate and communication success rate as examples. Reliability testing is conducted on unicast routing, multicast routing, and tree routing under different node packet loss rates. The results indicate that when the packet loss rate is below 50%, tree routing should be selected, and electromagnetic compatibility protection measures should be applied.

Acknowledgments

This work is supported by Science and Technology Project of State Grid Corporation of China Research on wide-band current array sensing technology for characterizing the operation state of main substation equipment (5200-202155419A-0-0-00).

References

[1] G. Behrmann and J. Smajic, "RF PD signal propagation in GIS: Comparing S-parameter measurements with an RF transmission model for a short section of GIS," in IEEE Transactions on Dielectrics and Electrical Insulation, vol. 23, no. 3, pp. 1331-1337, June 2016.

[2] H. Mohseni, J. Jadidian, A. A. Shayegani-akmal, E. Hashemi, A. Naieny and E. Agheb, "In-situ insulation test of 400 kV GIS," in IEEE Transactions on Dielectrics and Electrical Insulation, vol. 15, no. 5, pp. 1449-1455, October 2008.

[3] T. Wen, Y. Zhao, X. Fan, Q. Zhang, N. Shimomura and W. Chen, "Insulation characteristics of GIS bus with conductive protrusion attached to the high-voltage electrode under lightning impulses with different wavefront times," in IEEE Transactions on Dielectrics and Electrical Insulation, vol. 26, no. 6, pp. 1935-1940, Dec. 2019.

[4] T. Ito, M. Kamei, G. Ueta and S. Okabe, "Improving the sensitivity verification method of the UHF PD detection technique for GIS," in IEEE Transactions on Dielectrics and Electrical Insulation, vol. 18, no. 6, pp. 1847-1853, December 2011.

[5] J. Guo, J. -F. Zhang and Y. Zhao, "Adaptive Tracking Control of A Class of First-Order Systems With Binary-Valued Observations and Time-Varying Thresholds," in IEEE Transactions on Automatic Control, vol. 56, no. 12, pp. 2991-2996, Dec. 2011.

[6] L. Vu and D. Liberzon, "Supervisory Control of Uncertain Linear Time-Varying Systems," in IEEE Transactions on Automatic Control, vol. 56, no. 1, pp. 27-42, Jan. 2011.

[7] J. Lu, Q. Wei, Y. Liu, T. Zhou and F. -Y. Wang, "Event-Triggered Optimal Parallel Tracking Control for Discrete-Time Nonlinear Systems," in IEEE Transactions on Systems, Man, and Cybernetics: Systems, vol. 52, no. 6, pp. 3772-3784, June 2022.

[8] M. Ma, T. Wang, J. Qiu and H. R. Karimi, "Adaptive Fuzzy Decentralized Tracking Control for Large-Scale Interconnected Nonlinear Networked Control Systems," in IEEE Transactions on Fuzzy Systems, vol. 29, no. 10, pp. 3186-3191, Oct. 2021.

[9] L. Sun, J. Ma, H. Wang, Y. Zhang and J. Yong, "Cloud Service Description Model: An Extension of USDL for Cloud Services," in IEEE Transactions on Services Computing, vol. 11, no. 2, pp. 354-368, 1 March-April 2018.

[10] R. Garg, "MCDM-Based Parametric Selection of Cloud Deployment Models for an Academic Organization," in IEEE Transactions on Cloud Computing, vol. 10, no. 2, pp. 863-871, 1 April-June 2022.

Received 5 February 2024